Spin-wave dynamics for the high-magnetic-field phases of the frustrated CuFeO_{2} antiferromagnet: Predictions for inelastic neutron scattering

J. T. Haraldsen, R. S. Fishman, and G. Brown

Phys. Rev. B **86**, 024412 — Published 10 July 2012

DOI: 10.1103/PhysRevB.86.024412

Spin-wave dynamics for the high-magnetic-field phases of the frustrated $CuFeO_2$ antiferromagnet: Predictions for inelastic neutron scattering

J.T. Haraldsen[1,2], R.S. Fishman[3], and G. Brown[4]

[1] *Theoretical Division, Los Alamos National Laboratory, Los Alamos, NM 87545, USA*
[2] *Center for Integrated Nanotechnologies, Los Alamos National Laboratory, Los Alamos, NM 87545, USA*
[3] *Materials Science and Technology Division, Oak Ridge National Laboratory, Oak Ridge, TN 37831 and*
[4] *Department of Physics, Florida State University, Tallahassee, FL 32306*

We evaluate the spin-wave spectra for the high-field phases of the frustrated triangular lattice antiferromagnet with a focus on the observed high-magnetic field phases of $CuFeO_2$. After determining the appropriate magnetic ground state using a combination of Monte-Carlo simulations and variational methods for a two-dimensional triangular lattice, we evaluate the spin excitation frequencies and intensities using a rotational Holstein-Primakoff expansion for both the collinear and non-collinear states. These predictions should help experimentalists to identify the magnetic ground states of $CuFeO_2$ and other triangular-lattice antiferromagnets using inelastic neutron scattering.

PACS numbers: 78.70.Nx, 75.30.Ds, 75.10.Jm,75.30.Et

I. INTRODUCTION

Motivated by magnetically-induced electric polarization, a great deal of research has recently been devoted to understanding the possible ferroelectric/magnetic coupling mechanisms in "improper" multiferroics[1–5]. The competing interactions in these materials produce a wide range of collinear (CL) and non-collinear (NC) magnetic structures[5–10]. The ability to transverse those phases through doping or application of a magnetic field has provided an essential tool to understand these materials.

$CuFeO_2$ is a frustrated antiferromagnet that contains stacked triangular lattices[11]. Below about 7 T, the magnetic ground state of pure $CuFeO_2$ is a CL 4-sublattice (SL) ($\uparrow\uparrow\downarrow\downarrow$) phase. Above 7 T, it exhibits multiferroic behavior and is characterized by a complex non-collinear (CNC) state[12]. The CNC phase is also produced by Al or Ga doping, which decreases the easy-axis anisotropy[13,14] perpendicular to the hexagonal planes. Characterization of the CNC phase in Ga-doped $CuFeO_2$ shows that the magnetic structure is a distorted spiral with alternating small and large turn angles fluctuating between (19°-25°) and (130°-140°)[15,16]. While both the 4-SL and CNC phases of $CuFeO_2$ have been extensively investigated, the high-field phases are not well understood.

At about 13 T, the CNC phase transforms into a 5-SL phase[17], which does not exhibit multiferroic behavior possibly because it is commensurate. The 5-SL phase is stable up to about 20 T, above which a canted 3-SL phase becomes the ground state. At 34 T, the 3-SL phase smoothly transforms into a conical-type phase. A different conical phase appears at about 50 T[18–20]. Finally, all spins become aligned and the CL-1 (ferromagnetic) phase is reached at 70 T[22].

For materials like $CuFeO_2$ and $CuCrO_2$, the spin configurations in each hexagonal plane are stacked in an antiferromagnetic ($CuFeO_2$)[11] or ferromagnetic ($CuCrO_2$)[21] manner from one layer to the next. Because the interlayer interactions are not magnetically frustrated, the important behavior of these materials can be predicted based on a two-dimensional triangular-lattice antiferromagnet. An added advantage of $CuFeO_2$ is that the large $S = 5/2$ Fe^{3+} spins can be treated classically with a small error.

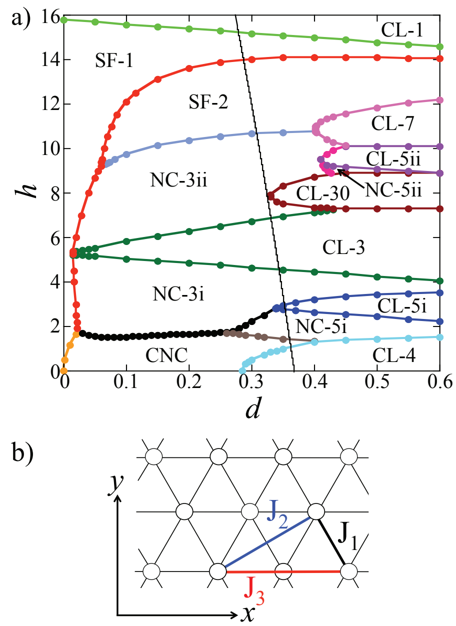

FIG. 1: (Color Online) (a) The magnetic phase diagram for the frustrated triangular lattice with $J_2/|J_1| = 0.4$ and $J_3/|J_1| = 0.75$ as determined by Ref. [23]. The black line indicates the proposed trajectory for $CuFeO_2$ with increased field and is given by h = 36.59-2.15d-255.64d^2. (b) The 2-D interactions considered for the frustrated triangular lattice consisting of J_1, J_2, and J_3.

Recently, the magnetic phase diagram of $CuFeO_2$ was predicted using a combination of variational and Monte-Carlo computational methods[23] on a two-dimensional lattice. As a function of magnetic field and anisotropy,

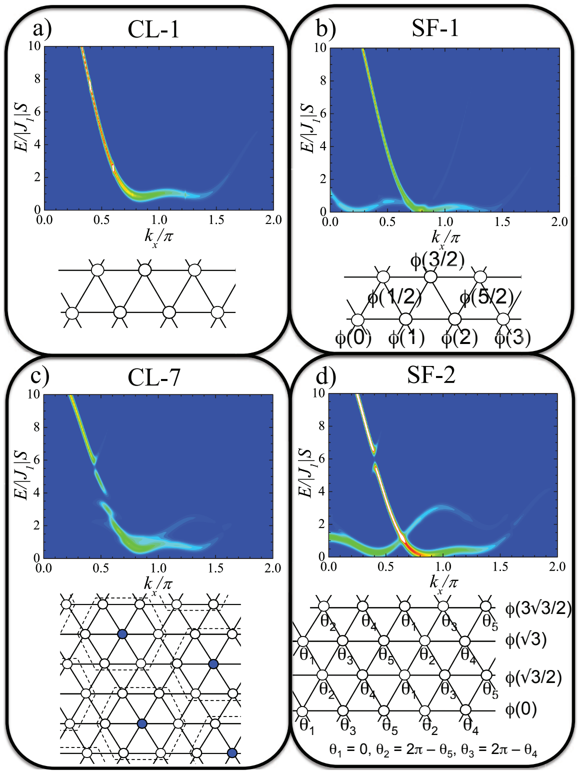

FIG. 2: (Color Online) The simulated spin-wave spectra along $\mathbf{k} = (k_x, 0)$ and spin configuration for the (a) CL-1 ($d = 0.5$ and $h = 16.0$), (b) SF-1 ($d = 0.290$ and $h = 14.467$), (c) CL-7 ($d = 0.5$ and $h = 11.0$), and (d) SF-2 ($d = 0.30$ and $h = 12.9$) phases[35].

the phase diagram was predicted to contain 14 possible phases (shown in Fig. 1(a)). The black line in Fig. 1(a) denotes the predicted trajectory for $CuFeO_2$ with increasing magnetic field, where anisotropy is assumed to decrease with magnetic field, as indicated experimentally[18,19].

In this report, we use a rotational Holstein-Primakoff expansion to evaluate the spin dynamics of the CL and NC spin structures for the high-field phases of the frustrated triangular lattice. In these calculations, we use the general interaction parameters determined for $CuFeO_2$. When possible, we follow along the predicted trajectory for $CuFeO_2$ to help explain the dynamical evolution of the spin-wave spectra for that material. Our goal and motivation is to provide experimentalists with a general idea of how the spin-wave frequencies and intensities evolve with magnetic field when investigating either $CuFeO_2$ or other frustrated triangular lattice materials.

II. 2-D FRUSTRATED TRIANGULAR LATTICE

The frustrated triangular lattice provides multiple interlayer super-exchange pathways (Fig. 1(b))[11,23,24]. Including both an external magnetic field and anisotropy, the Heisenberg Hamiltonian for a triangular lattice can be written as

$$H = -\frac{1}{2}\sum_{i\neq j} J_{ij}\mathbf{S}_i\cdot\mathbf{S}_j - D\sum_i \mathbf{S}_{iz}^2 - 2\mu_B H\sum_i \mathbf{S}_{iz}, \quad (1)$$

where $\mathbf{S}_i$ is the local moment on site i, D is the anisotropy energy, H is the external magnetic field, and the exchange coupling J_{ij} between sites i and j is antiferromagnetic when $J_{ij} < 0$. For convenience, we define $d = D/|J_1|$ and $h = 2\mu_B H/|J_1|S$ with all energies in units of J_1. Since all energies are in the units of J_1S, the INS spectra provided may be mapped on to other materials for a general understanding and identification of the phase dynamics. For convenience, we set the lattice constant to 1.

Candidate magnetic states were suggested by Monte-Carlo simulations on a 60×60 lattice. The precise ground states and their energies are found using a variational method on a large lattice. For incommensurate solutions, the spin state is expanded in harmonics of the ordering wavevector $\mathbf{Q} = Q_c\mathrm{x}$ as described in Refs. [23,24]. Based on the provided magnetic ground state, the spin-wave dynamics are evaluated using a Holstein-Primakoff transformation with the spin operators given by $S_{iz} = S - a_i^\dagger a_i$, $S_{i+} = \sqrt{2S}a_i$, and $S_{i-} = \sqrt{2S}a_i^\dagger$ (a_i and $a_i^\dagger$ are bosonic destruction and creation operators). The local spin operators are obtained from the laboratory spin operators by applying a rotation matrix[25,26]. Since higher order terms corresponding to spin-wave interactions and quantum fluctuations are unimportant at low temperatures and for small 1/S, they have been ignored in this analysis.

To determine the spin-wave frequencies $\omega_\mathbf{q}$, the equations-of-motion are solved for the vectors $\mathbf{v_q} = [a_\mathbf{q}^{(1)}, a_{-\mathbf{q}}^{(1)\dagger}, a_\mathbf{q}^{(2)}, a_{-\mathbf{q}}^{(2)\dagger}, ...]$, which may be written in terms of the $2N\times2N$ matrix $\underline{M}(\mathbf{q})$ as $id\mathbf{v_q}/dt = -[\underline{H}_2, \mathbf{v_q}] = \underline{M}(\mathbf{q})\mathbf{v_q}$, where N is the number of spin sites in the unit cell[25]. The spin-wave frequencies are then determined from the condition $\mathrm{Det}[\underline{M}(\mathbf{q}) - \omega_\mathbf{q}\underline{I}] = 0$, where all SW frequencies must be real and positive and all SW weights must be positive to assure the local stability of a magnetic phase.

The spin-wave intensities are determined by the coefficients of the spin-spin correlation function:

$$S(\mathbf{q},\omega) = \sum_{\alpha\beta}(\delta_{\alpha\beta} - q_\alpha q_\beta)S^{\alpha\beta}(\mathbf{q},\omega), \quad (2)$$

where α and β are x, y, or z[27]. A more detailed discussion of this method is contained in Ref. [25]. Notice that inelastic neutron-scattering (INS) measurements only detect components of the spin fluctuations perpendicular[28] to the wavevector $\mathbf{q}$.

The total intensity $I(\mathbf{q},\omega)$ for an INS scan at constant $\mathbf{q}$ is given by

$$I(\mathbf{q},\omega) = S(\mathbf{q},\omega)F_\mathbf{q}^2\exp\big(-(\omega-\omega_\mathbf{q})^2/2\delta^2\big), \quad (3)$$

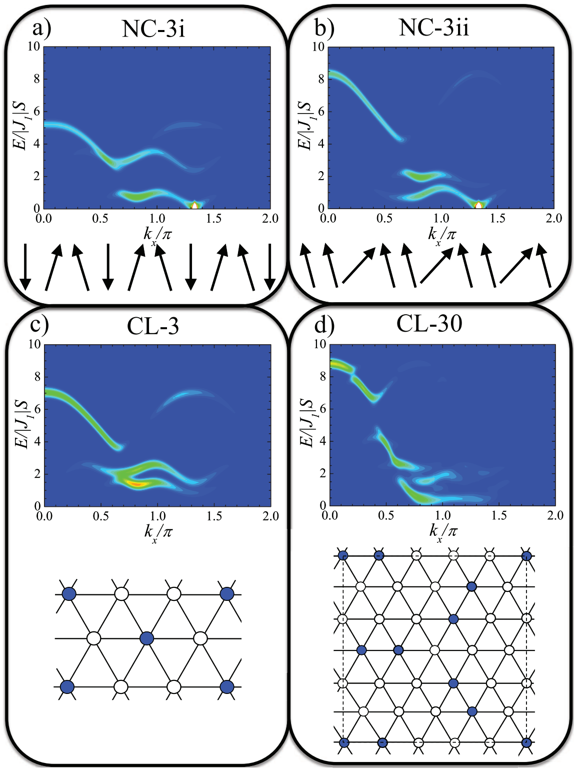

FIG. 3: (Color Online) The simulated spin-wave spectra along $\mathbf{k} = (k_x, 0)$ and spin configuration for the (a) NC-3i ($d = 0.355$ and $h = 3.61$), (b) NC-3ii ($d = 0.333$ and $h = 7.53$), (c) CL-3 ($d = 0.345$ and $h = 5.40$), and (d) CL-30 ($d = 0.5$ and $h = 7.0$) phases[35].

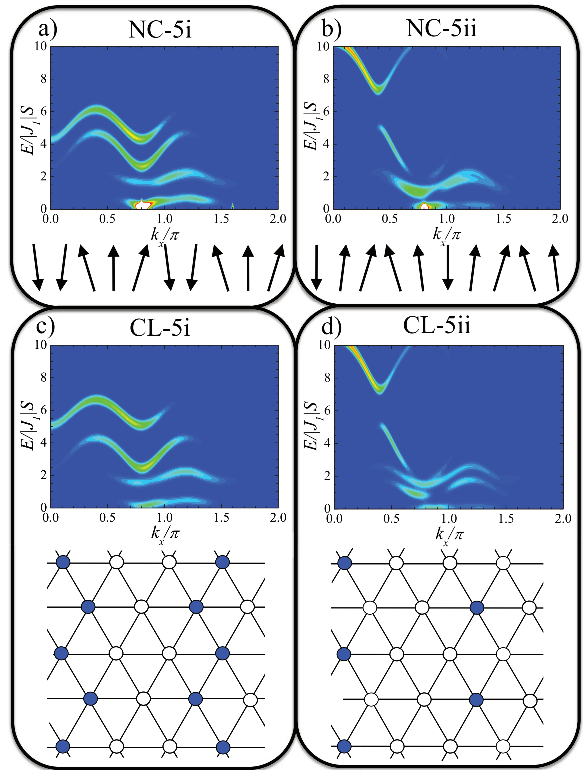

FIG. 4: (Color Online) The simulated spin-wave spectra along $\mathbf{k} = (k_x, 0)$ and spin configuration for the (a) NC-5i ($d = 0.303$ and $h = 2.12$), (b) NC-5ii ($d = 0.45$ and $h = 9.0$), (c) CL-5i ($d = 0.359$ and $h = 2.87$), and (d) CL-5ii ($d = 0.5$ and $h = 9.0$) phases[35].

where δ is the energy resolution and $F_{\mathbf{q}}$ is the Fe^{3+} ionic form factor given the interest in $CuFeO_2$[29,30]. The simulated energy resolution is based on a Gaussian distribution, which is standard for constant $\mathbf{q}$ scans on a triple-axis spectrometer[28,31]. Other experimental configurations may require more complex resolution functions.

It should be noted that the triangular lattice can produce "twin" branches of the spin state, with propagation wavevectors rotated by $\pm 60^\circ$ with respect to the main branch. The excitations of the "twin" branches will change the inelastic spectra along the k_x direction. However, the "twin" branches can be suppressed through the application of uniaxial pressure as shown in Ref. [32]. For clarity, the spin-wave dynamics described in this paper does not include the "twin" contributions.

III. PREDICTED SPIN DYNAMICS

Figure 1(a) presents the magnetic phase diagram for the frustrated triangular lattice with increasing anisotropy and magnetic field, which was determined using Monte-Carlo and variational techniques in Ref. [23]. The phase diagram contains multiple CL and NC phases (Fig. 1(a)) that are produced by the competition of the three exchange interactions (J_1, J_2, and J_3) as the anisotropy and external magnetic field are varied.

Generally, Fig. 1(a) indicates that the CL states are stabilized with increasing anisotropy. For $D >> J_1$, the spins become Ising-like without any transverse degrees of freedom. For zero field, the phase diagram of an Ising system with different exchange interactions J_2 and J_3 but $J_1 < 0$ was described evaluated by Takagi and Mekata[33]. As the anisotropy decreases, the incommensurate CNC phase[34] appears at low field. With increasing magnetic field, the CNC phase transforms into multiple NC and spin flop (SF) phases[23]. The SF-1 phase (Fig. 2(b)) is a conical phase with the same canting angle θ on every site and with a turn angle $\phi(x) = Q_1 x$ that varies linearly with x. The SF-2 phase (Fig. 2(d)) is more complicated with 5 sublattices in the x direction and a turn angle $\phi(y) = Q_2 y$ that increases linearly with y. More details on these phases are provided in Ref. [23].

In order to help experimentalists to identify these phases, we have simulated the INS dispersions along the $CuFeO_2$ trajectory given in Fig. 1(a). For comparison, phases not on the trajectory are also considered. Although we use the magnetic form factor for Fe^{3+}, the dispersion curves were evaluated for general S and are applicable to any material with stacked triangular lattices.

Generally, the spectra of the NC phases contain gapless Goldstone modes due to rotational invariance about the z axis. These modes would become gapped if we had also included easy-plane anisotropy, which breaks the rotational invariance by restricting the spins to the yz plane. By contrast, the easy-axis anisotropy D and the magnetic field H, both along the z axis, produce a spin-wave gap in the CL phases.

Figure 2 shows the INS dispersions along $\mathbf{k} = (k_x, 0)$ for the high-field ferromagnetic (a) CL-1 ($d = 0.5$ and $h = 16.0$), (b) SF-1 ($d = 0.290$ and $h = 14.467$), (c) CL-7 ($d = 0.5$ and $h = 11.0$), and (d) SF-2 ($d = 0.30$ and $h = 12.9$) phases[35]. Since these phases are close to the field-induced ferromagnetic phase, their excitation spectra are very similar. Therefore, subtle details in the dispersions are important. For the SF phases, two dispersive modes appear. Compared to the CL-1 spectrum, the spectra of the SF and CL-7 phases all show distinct signatures that should help to identify them using INS. While the CL-1 phases presents a smooth continuous dispersion, the CL-7 and SF-2 phases have "breaks" in their dispersions around $\mathbf{k} = (\pi/2, 0)$ and the SF-1 phase has two modes that mirror each other at $\mathbf{k} = (4\pi/5, 0)$.

In Fig. 3, we present the INS dispersions along $\mathbf{k} = (k_x, 0)$ for the (a) NC-3i ($d = 0.355$ and $h = 3.61$), (b) NC-3ii ($d = 0.333$ and $h = 7.53$), (c) CL-3 ($d = 0.345$ and $h = 5.40$), and (d) CL-30 ($d = 0.5$ and $h = 7.0$)[35]. While the NC 3-SL spectrum exhibits a Goldstone mode at $\mathbf{k} = (4\pi/3,0)$, the CL-3 and CL-30 spectra are gapped systems.

Figure 4 shows the INS dispersions along $\mathbf{k} = (k_x, 0)$ for the (a) NC-5i ($d = 0.303$ and $h = 2.12$), (b) NC-5ii ($d = 0.45$ and $h = 9.0$), (c) CL-5i ($d = 0.359$ and $h = 2.87$), and (d) CL-5ii ($d = 0.5$ and $h = 9.0$)[35]. Similar to the 3-SL phases, the NC-5i and NC-5ii spectra have Goldstone modes at $\mathbf{k} = (4\pi/5,0)$, but the spectra of the CL phases are gapped with minima at the same wavevector as the NC Goldstone mode.

IV. DISCUSSION

Following the predicted trajectory for $CuFeO_2$, distinct changes in the spin-wave dispersions are produced by the competition between the field and anisotropy energies. Once the CL-4 and CNC phases are passed, the system enters the NC-5i phase (Fig. 4(a)), which has a Goldstone mode at $\mathbf{k} = (4\pi/5\ ,0)$. As the field is increased further, this mode becomes slightly gapped in the CL-5i phase (Fig. 4(c)). However, the main signatures of the NC-5i and CL-5i phases remain the same.

The NC-5i phase may be distinguished from the CL-5i phase by the dependence of the gap on field. Since the NC phase has a gapless Goldstone mode but the CL phase does not, INS would observe a decrease in the Goldstone mode intensity as the field is increased. The spin-wave gap that appears in the CL-5i phase will increase linearly with field. Magnetization and diffraction measurements[13,14] strongly suggest that the NC-5i phase appears above the CNC phase in doped samples: the wavevector $\mathbf{k} = (4\pi/5,0)$ of the 5-SL phase remains constant while the magnetization linearly increases with field. INS measurements can be used to confirm the appearance of the NC-5i phase in those materials.

It should be noted that the CL-5i phase also has a local minima at approximately $\mathbf{k} = (4\pi/3,0)$. This provides a precursor to the NC-3i phase (Fig. 3(a)), since the spectral weight shifts to the Goldstone mode of the NC-3i phase at $\mathbf{k} = (4\pi/3,0)$.

As the magnetic field grows larger, the spin-waves becomes gapped again in the CL-3 phase (Fig. 3(c)). While one mode is raised in energy by the magnetic field, a second mode is lowered in energy by the reduced anisotropy. The anisotropy dominates over the magnetic field and restores the Goldstone mode as the system enters the NC-3ii phase (Fig. 3(b)). As the magnetic field increases further, the system becomes gapped again as the system transforms into the SF-2 phase (Fig. 2(d)). This phase then smoothly transforms into the SF-1 phase (Fig. 2(b)). The leftmost mode of the SF-1 phase becomes less intense and disappears as the system enters the CL-1 phase (Fig. 2(a)). In the fully aligned CL-1 phase, the dispersion simply increases with field.

An animation of these modes along the $CuFeO_2$ trajectory is provided in the supplementary material[36]. This movie visually depicts the changes in the spin-wave frequencies and intensities just described. Specifically, the movie shows how the intensity of the Goldstone mode in the NC-5i phase changes with increasing field.

Since the modes of each magnetic phase have specific characteristic features, INS is a critical tool to distinguish between those phases. This is particularly evident in the case of the 5SL phases of $CuFeO_2$ (NC-5i - Fig. 4(a) and CL-5i - Fig. 4(c)) since both phases have the same wavevector and the magnetization provides only a qualitative distinction between the CL and NC phase. By probing the local degrees of freedom[28], INS provides a "dynamical fingerprint" of the underlying magnetic structure. Correspondingly, predictions of the spin-wave dynamics are critical for the interpretation of INS spectra and the identification of collinear and non-collinear magnetic phases for magnetic materials.

V. CONCLUSION

In conclusion, we predict the spin-wave dynamics for the high-field phases of a frustrated triangular lattice with focus on the parameter space for the multiferroic $CuFeO_2$ for comparison to future experiments. This calculations were performed using a rotational Holstein-Primakoff expansion for both the CL and NC phases. Analysis of the spin-wave spectra for these phases shows the constant competition between the magnetic field and the anisotropy energies. It is a goal of this paper that these predictions can be used to help experimentalists identify the high-field phases for $CuFeO_2$ or the phases for other triangular-lattice antiferromagnets like $CuCrO_2$.

VI. ACKNOWLEDGEMENTS

Research by JTH supported by the Center for Integrated Nanotechnologies, a U.S. Department of Energy, Office of Basic Energy Sciences user facility. Los Alamos National Laboratory, an affirmative action equal opportunity employer, is operated by Los Alamos National Security, LLC, for the National Nuclear Security Administration of the U.S. Department of Energy under contract DE-AC52-06NA25396. Research by RF sponsored by the U.S. Department of Energy, Office of Basic Energy Sciences, Materials Sciences and Engineering Division. GB acknowledges computer time provided by Florida State University.

[1] T. Kimura, T. Goto, H. Shintani, K. Ishizaka, T. Arima, and Y. Tokura, Nature (London) **426**, 55 (2003).
[2] D.I. Khomskii, Magn. Magn. Mater **306**, 1 (2006).
[3] S.-W. Cheong, and M. Mostovoy, Nature Materials **6**, 13 (2007).
[4] R. Ramesh, and N. A. Spaldin, Nature Materials **6**, 21 (2007).
[5] W. Eerenstein, N.D. Mathur, and J.F. Scott, Nature **442**, 759 (2006).
[6] H. Katsura, N. Nagaosa, and A. V. Balatsky, Phys. Rev. Lett. **95**, 057205 (2005).
[7] M. Mostovoy, Phys. Rev. Lett. **96**, 067601 (2006).
[8] I. A. Sergienko and E. Dagotto, Phys. Rev. B **73**, 094434 (2006).
[9] T. Arima, J. Phys. Soc. Jpn. **76**, 073702 (2007).
[10] M. Soda, K. Kimura, T. Kimura, M. Matsuura, and K. Hirota, J. Phys. Soc. Jpn. **78**, 124703 (2009).
[11] R.S. Fishman, F. Ye, J.A. Fernandez-Baca, J.T. Haraldsen, and T. Kimura, Phys. Rev. B **78**, 140407(R) (2008).
[12] T. Kimura, J. C. Lashley, and A. P. Ramirez, Phys. Rev. B **73**, 220401(R) (2006).
[13] S.Seki, Y. Yamasaki, Y. Shiomi, S. Iguchi, Y. Onose, and Y. Tokura, Phys. Rev. B **75**, 100403(R) (2007).
[14] S. Kanetsuki, S. Mitsuda, T. Nakajima, D. Anazawa, H. A. Katori, and K. Prokes, J. Phys.: Condens. Matter **19**, 145244 (2007).
[15] J.T. Haraldsen, F. Ye, R. S. Fishman, J.A. Fernandez-Baca, Y. Yamaguchi, K. Kimura, and T. Kimura, *Phys. Rev. B.* **82**, 020404(R) (2010).
[16] J. T. Haraldsen and R. S. Fishman, *Phys. Rev. B* **82**, 144441 (2010).
[17] S. Mitsuda, M. Mase, K. Prokes, H. Kitizawa, and H.A. Katori, J. Phys. Soc. Japan **69**, 3513 (2000).
[18] N. Terada, Y. Narumi, Y. Sawai, K. Katsumata, U. Staub, Y. Tanaka, A. Kikkawa, T. Fukui, K. Kindo, T. Yamamoto, R. Kanmuri, M. Hagiwara, H. Toyokawa, T. Ishikawa, and H. Kitamura, Phys. Rev. B **75**, 224411 (2007).
[19] T.T.A. Lummen, C. Strohm, H. Rakoto, A.A. Nugroho, and P.H.M. van Loosdrecht, Phys. Rev. B **80**, 012406 (2009).
[20] G. Quirion, M.L. Plumer, O.A. Petrenko, G. Balakrishnan, and C. Proust, Phys. Rev. B **80**, 064420 (2009).
[21] M. Frontzek,J. T. Haraldsen, A. Podlesnyak, M. Matsuda, A. D. Christianson, R. S. Fishman, A. S. Sefat, Y. Qiu, J. R. D. Copley, S. Barilo, S. V. Shiryaev, and G. Ehlers, Phys. Rev. B **84**, 094448 (2011).
[22] Y. Ajiro, T. Asano, T. Takagi, M. Mekata, H.A. Katori, and T. Goto, Physica B **201**, 71 (1994).
[23] R. S. Fishman, G. Brown, and J. T. Haraldsen, Phys. Rev. B **85**, 020405(R) (2012).
[24] R.S. Fishman and S. Okamoto, Phys. Rev. B. **81**, 020402(R) (2010).
[25] J. T. Haraldsen and R.S. Fishman, J. Phys.: Condens. Matter **21**, 216001 (2009).
[26] M.E. Zhitomirsky and I.A. Zaliznyak, Phys. Rev. B **53** 3428 (1996).
[27] G. L. Squires, *Introduction to the Theory of Thermal Neutron Scattering* (Dover Publications, New York, 1978).
[28] G. Shirane, S. M. Shapiro, and J. M. Tranquada, *Neutron Scattering with a Triple-Axis Spectrometer* (Cambridge University Press, Cambridge, 2002).
[29] The Fe^{3+} magnetic form factor is given as $F_{\mathbf{q}} = j_0(\mathbf{q})$, where $j_0(\mathbf{q}) = A_0 e^{a_0 s^2} + B_0 e^{b_0 s^2} + C_0 e^{c_0 s^2} + D_0$ and $s = \sin\theta/\lambda = q/4\pi$. The coefficients are $A_0 = 0.3972$ ($a_0 = 13.2442$), $B_0 = 0.6295$ ($b_0 = 4.9034$), $C_0 =$ -0.0314 ($c_0 = 0.3496$), and $D_0 = 0.0044$ from Ref. [30].
[30] A.J. Dianoux and G. Lander, *Neutron Data Booklet* (OCP Science, Philadelphia, 2003).
[31] N. J. Chesser and J. D. Axe, *Acta Cryst. A* **29**, 160 (1973).
[32] T. Nakajima, S. Mitsuda, J. T. Haraldsen, R. S. Fishman, T. Hong, N. Terada, Y. Uwatoko, Phys. Rev. B **85**, 144405 (2012).
[33] T. Takagi and M. Mekata, *J. Phys. Soc. Jpn.* **64**, 4609 (1995).
[34] J. T. Haraldsen, M. Swanson, G. Alvarez, and R. S. Fishman, Phys. Rev. Lett. **102**, 237204 (2009).
[35] The conical SF-1 phase ($d = 0.29$ and $h = 14.467$) consists of $\theta = 0.0992\pi$ and $Q_1 = 0.846\pi$. The SF-2 phase($d = 0.30$ and $h = 12.9$) has turn angles $\theta_1 = 0.0$, $\theta_2 = 0.13646\pi$, $\theta_3 = 1.7534\pi$, $\theta_4 = 0.2466\pi$, and $\theta_5 = 1.8635\pi$ with $Q_2 = 0.42731\pi$. The NC-3i phase ($d = 0.355$ and $h = 3.6$) has turn angles $\theta_1 =$ -0.13989π, $\theta_2 =$ -π, $\theta_3 = 0.13989\pi$. The NC-3ii phase ($d = 0.333$ and $h = 7.53$) has turn angles $\theta_1 =$ -0.11616π, $\theta_2 =$ -0.11616π, and $\theta_3 = 0.69698\pi$. The NC-5i ($d = 0.303$ and $h = 2.12$) consists of turn angles $\theta_1 = 0.0$, $\theta_2 = 1.8485\pi$, $\theta_3 = 1.0437\pi$, $\theta_4 = 0.95631\pi$, and $\theta_5 = 0.15149\pi$. The NC-5ii ($d = 0.45$ and $h = 9.0$) has turn angles $\theta_1 = \pi$, $\theta_2 = 0.0726\pi$, $\theta_3 = 0.02174\pi$, $\theta_4 = 1.9782\pi$, and $\theta_5 = 1.9273\pi$.
[36] Supplementary Material can be found at URL *www.needstobeadded*